TÜBİTAK

Turkish Journal of Chemistry

http://journals.tubitak.gov.tr/chem/

Research Article

Turk J Chem
(2022) 46: 394-403
© TÜBİTAK
doi:10.3906/kim-2110-45

In situ prepared tungsten(VI) oxide supported Pd0 NPs, remarkable activity and reusability in H2 releasing from dimethylamine borane

Seda KARABOĞA*
Department of Chemistry, Faculty of Arts and Science, Bolu Abant İzzet Baysal University, Bolu, Turkey

Received: 20.10.2021 • **Accepted/Published Online:** 25.11.2021 • **Final Version:** 27.04.2022

Abstract: The study reports preparation, characterization, and catalytic activity of Pd^0/WO_3 nanoparticles in H_2 evolution from dimethylamine borane (DMAB). The active catalyst called Pd^0/WO_3 NPs were obtained from the in situ reduction of Pd^{2+}/WO_3 precatalyst and tested in H_2 releasing from DMAB. Pd^0/WO_3 NPs were found as remarkable catalysts providing a turnover frequency value of 948.0 h^{-1} in H_2 releasing from DMAB at 60.0 ± 0.5 **°C**. The results of some advanced analytical techniques reveal that Pd^0 NPs show uniform dispersion on the surface of tungsten(VI) oxide (WO_3) with 5.85 ± 0.57 nm of particle size. The reducible nature of tungsten(VI) oxide improves the catalytic efficiency of Pd^0/WO_3 NPs in H_2 generation from DMAB. Pd^0/WO_3 NPs were found as active catalysts even after the 6th run of dehydrogenation reaction. The report also covers the kinetic performance of the catalyst.

Key words: Pd^0 Nanoparticles, tungsten(VI) Oxide, dehydrogenation, dimethylamine Borane, heterogeneous Catalyst.

1. Introduction

In the future of sustainable energy, the usage of hydrogen as an energy carrier to store energy appears inevitable. Hydrogen being a clean, sustainable, and efficient energy carrier is one of the appropriate candidates for the storage of energy [1]. It is stored energy as chemically, transport energy and used as a fuel [2]. The hydrogen based energy system called hydrogen economy is an advanced technology system [3]. It is possible to provide sustainable energy using this policy without polluting the environment. However, the safe storage of hydrogen in systems where it will be used as an energy carrier is important and to overcome obstacles in this regard. In recent years, boron compounds are suitable candidates for solid hydrogen storage materials such as ammonia borane, hydrazine borane, and dimethylamine borane [4,5,6]. Among the solid hydrogen storage materials, dimethylamine borane (DMAB, $(CH_3)_2NH.BH_3$) is a prominent B-N compound [7]. In the presence of a suitable catalyst, one equivalent of hydrogen could be released from dimethylamine borane [5,8,9] (Equation1).

$$2(CH_3)_2NH{-}BH_3 \xrightarrow{catalyst} \begin{matrix}(H_3C)_2N{-}BH_2\\ |\quad\quad |\\ H_2B{-}N(CH_3)_2\end{matrix} + 2H_2 \qquad (1)$$

The rate of hydrogen evolution depends on metal catalysts used in dehydrogenation reactions [10, 11]. Among transition metal nanoparticles, especially ruthenium has been used as a catalyst in dehydrogenation reactions [10,12,13,14,15] . However, there are few reports on the usage of palladium based on heterogeneous catalyst in H2 evolution from DMAB: three of them are monometallic [16,17,18] and five of them are bimetallic [19,20,21,22] or trimetallic [23] that act as heterogeneous catalysts. The main problem of the metal nanoparticles acting as the active catalyst is that they are not stable as thermodynamically during the reaction and they tend to be agglomerate. So, they need supporting materials to prevent the agglomeration of the metal nanoparticles. WO3 being one of the suitable supporting materials for transition metal nanoparticles has been used in various reactions such as oxidation of methanol and ethanol [24,25], dehydrogenation of 2-butanol [26], hydrolysis of ammonia borane [27], decomposition of formic acid [28]. Herein, WO3 was used as a supporting material for palladium(0) nanoparticles due to its reducible nature. WO3 can readily go to reduction under reaction conditions and this situation leads to the excess negative charge on the surface which enhances the catalytic performance of the catalyst depending on strong interaction between metal and support [28]. This unique property of WO3 gives a special chance that it could be used several types of reactions. Palladium(II) acetylacetonate was used as

* Correspondence: tanyildizi_s@ibu.edu.tr

a precursor and impregnated on the surface of the WO3. The precatalyst, Pd2+/WO3 was trialed in dehydrogenation of dimethylamine borane. The reduction of Pd2+ ions on the surface of WO3 leads to Pd0/WO3 which act as an active catalyst during the reaction course. Pd0/WO3 NPs are found as active catalysts providing a turnover frequency value of 948.0 h-1 in H2 evolution from DMAB at 60.0 ± 0.5 °C. The reusability tests showed that Pd0/WO3 NPs are tremendously stable catalysts even after the 6th run of dehydrogenation reaction. The Pd0/WO3 catalyst was collected from the reaction medium and characterized by XRD, TEM, XPS techniques. The study also covers the kinetic performance of the catalyst.

2. Experimental

2.1. Materials

Palladium(II) 2,4-pentanedionate ($Pd(C_5H_7O_2)_2$), toluene, and dimethylamine borane ($((CH_3)_2NH.BH_3$, 97%) were purchased from Aldrich. Tungsten(VI) oxide (WO_3, 99.9%) was bought from Nanografi. The glassware used in dehydrogenation reactions was cleaned with acetone and dried in an oven for 12 h.

2.2. Instrumentation

The instrumentation part is the same as the one given in our previous work, except for TEM analysis [11]. TEM images were obtained by Hitachi HT-7700 operating at 120kV.

2.3. In situ preparation of Pd^0/WO_3 NPs in H_2 generation reactions

Pd^0/WO_3 NPs were obtained from the in situ reduction of Pd^{2+} ions on the surface of support during the catalytic reaction. In this method, Pd^{2+} ions and supporting material, WO_3 were mixed for 1 h to adherence to Pd^{2+} ions. A 2.91 mM stock solution of palladium(II) acetylacetonate was prepared by dissolving 8.85 mg Pd(II) acetylacetonate in 10.0 mL of toluene. The defined amount of the stock solution was transposed to the reactor including 100.0 mg of WO_3 and stirred at 25.0 ± 0.5 °C for 1 h. The temperature of the mixture was fixed at 60 °C by circulating the water around the reaction tube. Then, DMAB was added to the reactor and hydrogen evolution was followed by measuring the water level inside the glass tube.

2.4. Determination of catalytic performance of Pd^0/WO_3 NPs with different palladium loadings.

In order to determine the optimum Pd loading in the catalyst sample, a series of experiments were performed using 100 mg WO_3 with different Pd loadings (0.5, 1.0, 1.5, and 2.0 % wt. Pd) in 10 mL of a toluene solution. 100 mM DMAB (60.10 mg) was used for each experiment. The highest turnover frequency value was obtained for 1.0% Pd wt. and found as 948.0 h^{-1} at 60.0 ± 0.5 °C in H_2 generation reaction. Therefore, Pd^0/WO_3 NPs with 1.0% Pd loading were used for further dehydrogenation experiments.

2.5. Leaching test of Pd^0/WO_3 NPs catalyst in H_2 generation reaction

After the first run of reaction, the reaction tube was settled down to the collapse of the catalyst. Then, the liquid part of the solution was filtered by using a feeding tube and collected. The filtrate part and solid part of the sample were separately tested in hydrogen releasing from DMAB. While the liquid part of the sample does not indicate any catalytic activity, the solid part is still active in the reaction.

2.6. Recyclability test for Pd^0/WO_3 in H_2 generation reaction

The catalytic activity of Pd^0/WO_3 NPs was tested in subsequent runs of dehydrogenation reaction. After the first run of the reaction, the same amount of DMAB was added to the reaction solution and the reaction was followed. The same experimental procedure was repeated for the subsequent runs.

3. Results and discussion

3.1. Characterization of Pd^0/WO_3 NPs

After determination of catalytic efficiency of Pd^0/WO_3 NPs, they were characterized by analytical techniques such as XRD, TEM, and XPS. Figure 1 shows the XRD patterns of bare WO_3 and WO_3 supported Pd^0 NPs after the catalytic dehydrogenation reaction of DMAB. No significant change has been seen in WO_3 crystallinity after Pd loading on the surface of the support. There is no additional peak that belongs to metallic Pd in XRD pattern in Figure 1 due to the low Pd loading in the sample. (PDF Card No: 01-083-0950).

TEM images of Pd^0/WO_3 NPs given in Figure 2 depict that Pd^0 NPs are well dispersed on the surface of WO_3. The mean particle size of Pd^0 NPs supported on the surface of WO_3 was determined from the TEM images by measuring more than 150 nontouching particles on the images. The histogram in Figure 2c shows the particle size distribution of Pd^0 NPs. WO_3 supported Pd^0 NPs are well dispersed on the support with an average particle size of 5.85 ± 0.57 nm.

The survey scan XPS analysis and high resolution spectra of Pd^0/WO_3 sample could be seen in Figure 3. The survey scan spectrum of Pd^0/WO_3 NPs shows that Pd, W, O and C existed in the sample (Figure 3a). For Pd, deconvolution of Pd 3d photoelectrons was obtained as seen in Figure 3b. The high resolution spectra of Pd 3d scan of Pd^0/WO_3 sample indicates

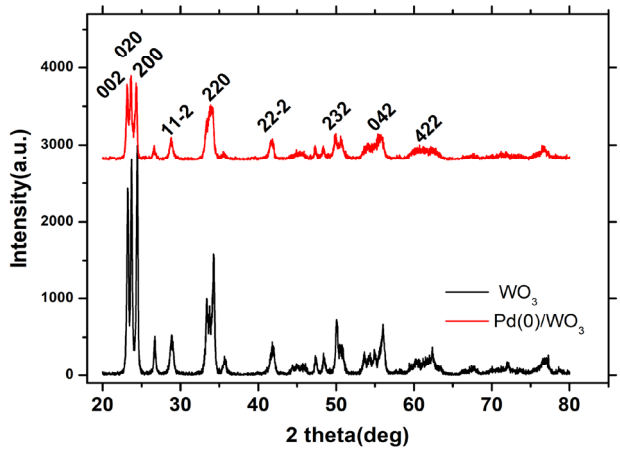

Figure 1. XRD pattern of bare WO_3 and 1.0% Pd wt. loaded WO_3 samples.

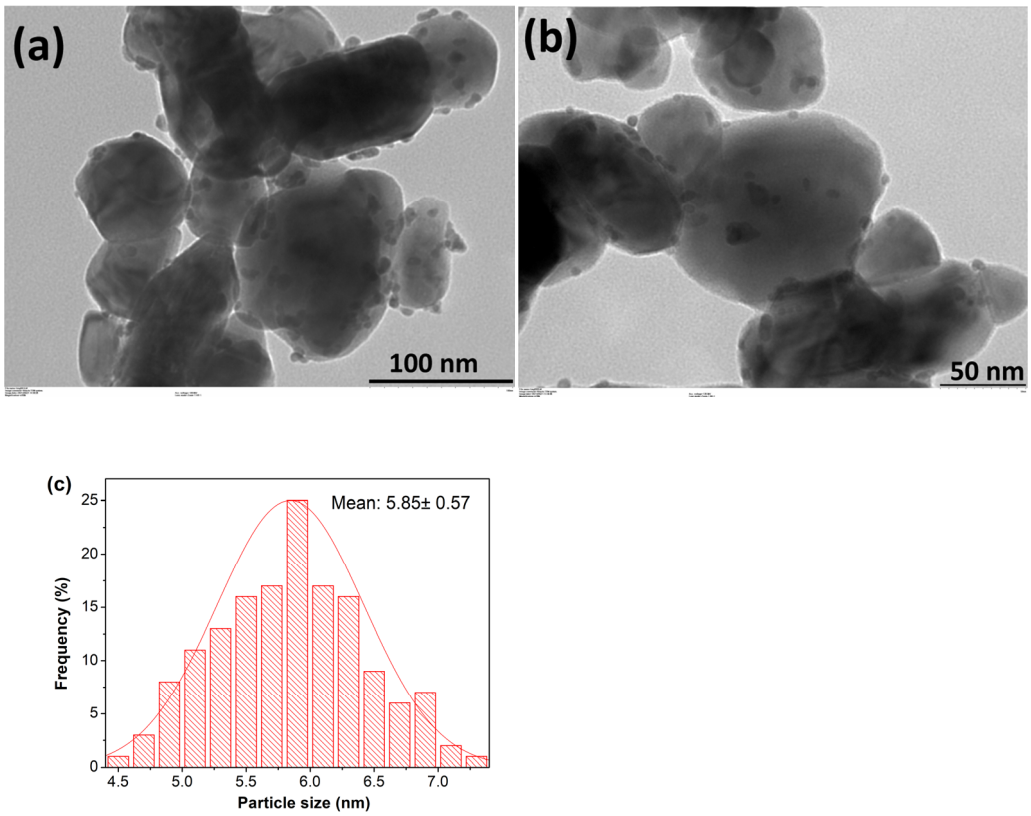

Figure 2. a, b) TEM images of WO_3 supported Pd^0 NPs with 1.0% Pd wt. c) Particle size diagram of Pd^0 NPs on the surface of WO_3.

two main peaks at 343.8 and 340.0 eV which could be attributable to $3d_{5/2}$ and $3d_{3/2}$ of metallic palladium, respectively [29,30]. The peaks at higher binding energy may be attributed to Pd being in a 2+ oxidation state [31,32]. The two peaks with low intensity have resulted from the oxidation of palladium metal in Pd^0/WO_3 sample during the XPS analysis. The color of WO_3 turns dark blue during the reaction course, which indicates the reduction of W^{6+} to W^{5+} with the addition of DMAB. However, well fitted W4f core-level XPS spectrum in Figure 3c indicates that no noticeable peak for W^{5+} state due to the oxidation of sample subjugated to air during the sampling.

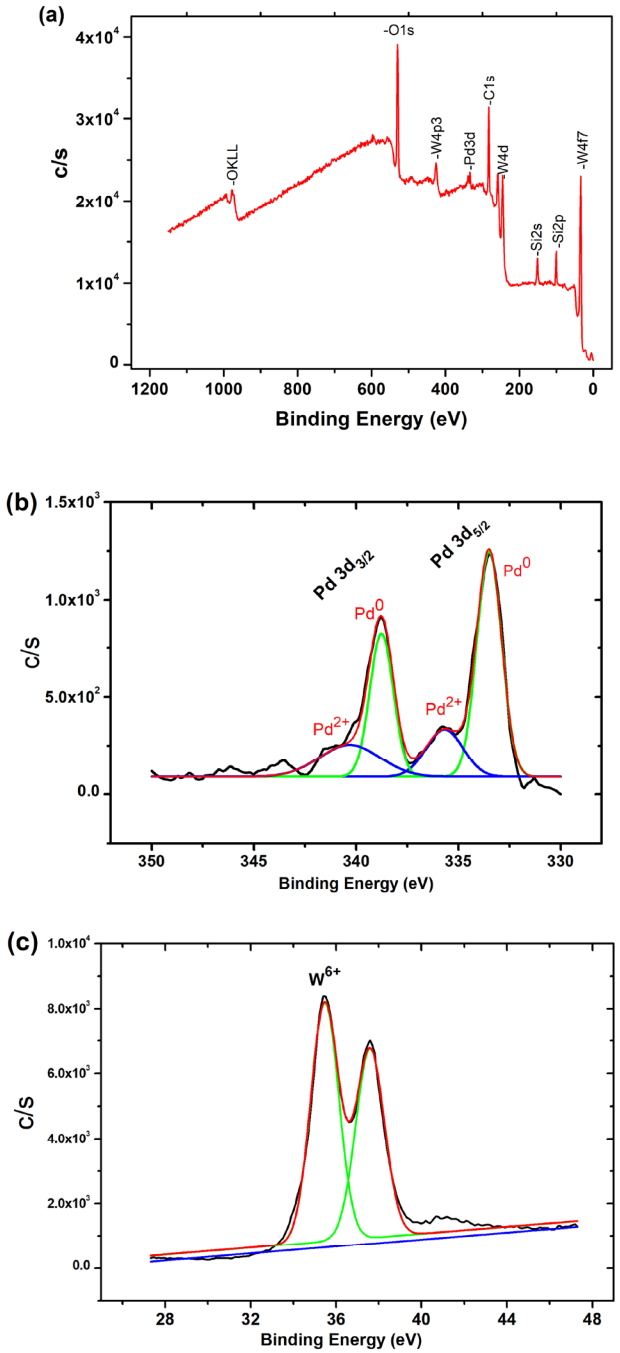

Figure 3. XPS spectra of Pd^0/WO_3 sample. a) Full range XPS spectra, b) Deconvolution of Pd 3d range, c) XPS spectrum of $W4f_{7/2}$ bands.

3.2. Catalytic performance of Pd^0/WO_3 NPs

Hydrogen evolution from DMAB was investigated in the presence of Pd^0/WO_3 NPs catalyst. Before testing the Pd^0/WO_3 NPs, bare Pd^0 NPs were tested in hydrogen releasing from DMAB at 60.0 ± 0.5 °C. The comparison of bare Pd^0 NPs and WO_3 supported Pd^0 NPs given in Figure 4 shows that WO_3 enhances the catalytic activity of Pd^0 NPs owing to prevent the agglomeration of them during the reaction course. The catalytic performance of Pd^0/WO_3 NPs changes depending on palladium loadings in the sample. Figure 5a indicates the hydrogen evolution varying with palladium loadings of the $Pd^0/$

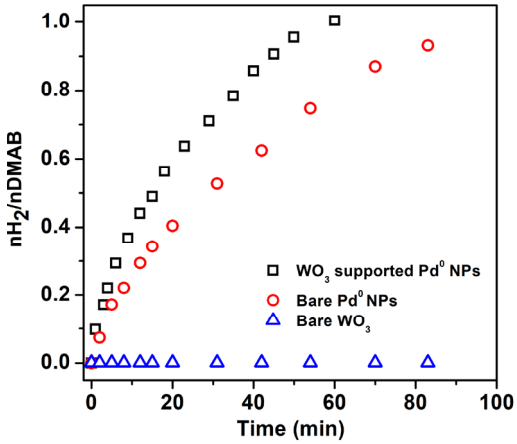

Figure 4. Comparison of hydrogen evolution from DMAB in the presence of bare Pd^0 NPs and WO_3 supported Pd^0 NPs.

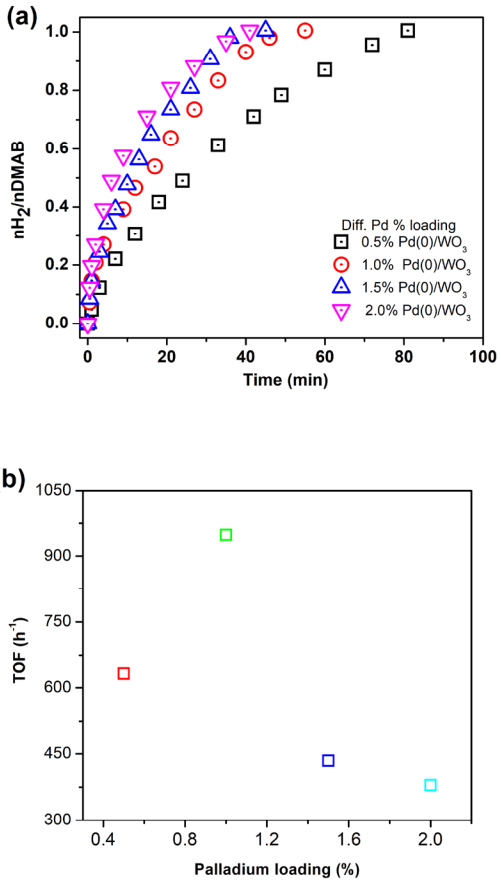

Figure 5. a) H_2 evolution graph with different Pd loadings (0.5, 1.0, 1.5, and 2.0 % wt.) b) TOF vs Pd loading in the catalyst.

WO_3 sample at 60.0 ± 0.5 °C. Hydrogen evolution rates and initial TOF values vary depending on palladium loading in the catalyst. The highest turnover frequency was found as 948 h^{-1} for 1.0% Pd wt loading of Pd^0/WO_3 sample. Figure 5b depicts palladium loading versus the TOF value of the catalyst. The volcano shape of the graph describes the relationship needed

to be optimized between the palladium and WO_3 support. The TOF value reaches a maximum and then decreases with the increment of palladium loading which is related to the supporting capacity of WO_3 support and agglomeration of Pd^0 NPs on the surface of the support. This type of relation has been previously reported for copper and palladium catalyst in hydrogen generation reactions [11, 16]. Therefore, Pd^0/WO_3 NPs with 1.0% wt Pd were used for further experiments.

Dehydrogenation reactions were performed with different catalyst concentrations to determine the reaction order with respect to catalyst. Figure 6a shows hydrogen evolution from DMAB in the presence of Pd^0/WO_3 NPs with different palladium concentrations. Hydrogen evolution rate was determined by the linear part of each line and the slope of the line was found as 0.86 indicating that dehydrogenation of DMAB is approximately first order with respect to palladium catalyst concentration (Figure 6b).

The effect of substrate concentration was also determined by performing a set of experiment while keeping the metal concentration constant at 0.95 mM. It can be seen that from the slope of the line in Figure 6c, the hydrogen generation rate from the catalytic dehydrogenation of DMAB is actually independent of DMAB concentration. So, the reaction catalyzed by $Pd(0)/WO_3$ NPs is zero order with respect to the substrate concentration (Figure 6d). Thus, the rate law of dehydrogenation reaction can be given as Eq 2:

$$\text{Rate} = k^{app}[Pd]$$

H_2 production reactions were studied at various temperatures (Figure 7a). The activation energy of the catalytic dehydrogenation of DMAB was determined from the slope of Arrhenius plot [33] to be Ea = 77.84 kJ/mol which is comparable to the previously reported values [18, 20, 21].

Recyclability of the catalyst is very important as well as catalytic activity in terms of practical applications. Recyclability of Pd^0/WO_3 NPs was performed in the dehydrogenation of DMAB at 60.0 ± 0.5 °C and it is seen in Figure 8 that Pd^0/WO_3 NPs are still impressive catalysts after the 6th run of the reaction. The special property of WO_3 support undergoing reduction in suitable conditions plays a significant role in the catalytic usage of Pd^0 NPs in H_2 evolution reactions. The reducibility feature of WO_3 leads to a partial reduction of W6+ to W5+ and excessive charge on the surface of support which promotes the strong interaction between metal and support.

Leaching experiment and poisoning experiments were also studied for Pd^0 NPs supported on the surface of WO_3. After the first run of the catalytic run, the reaction solution was filtered by inverse filtration using a feeding tube and

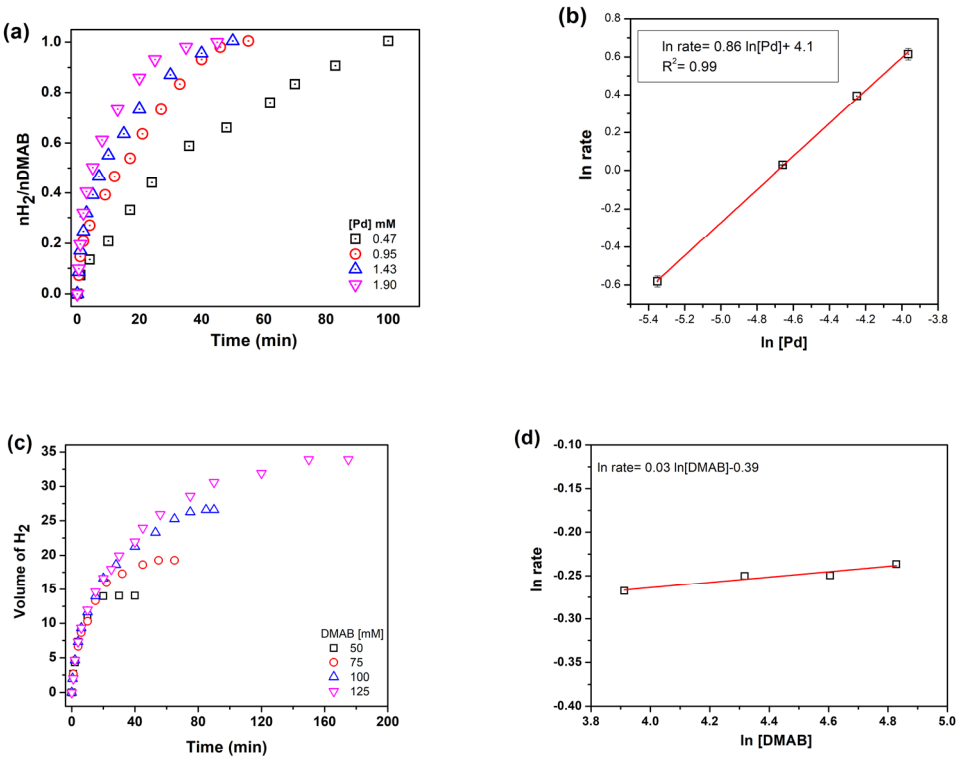

Figure 6. a) H2 evolution graph with different Pd concentrations b) ln rate vs. ln Pd c) Hydrogen evolution graph with different DMAB concentrations d) ln rate vs. ln DMAB.

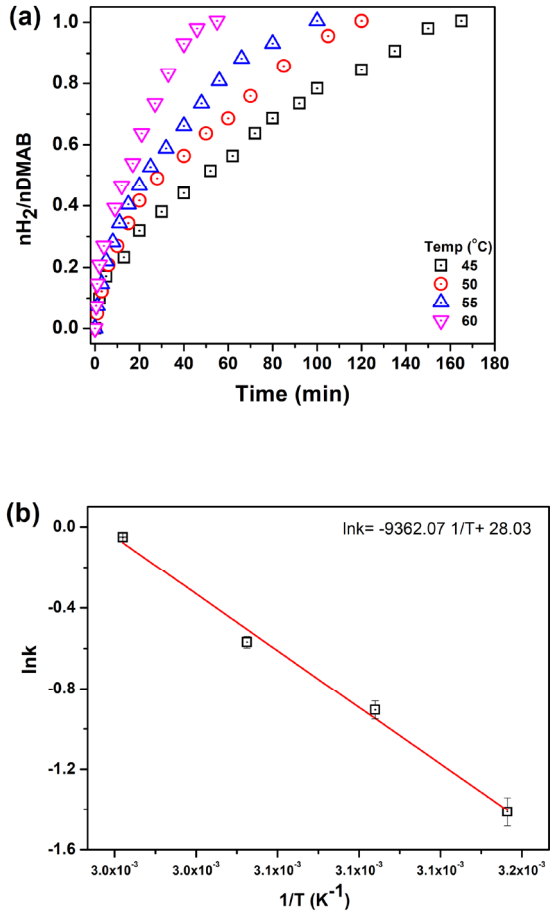

Figure 7. a) H_2 evolution from DMAB at different temperatures, b) Arrhenius plot.

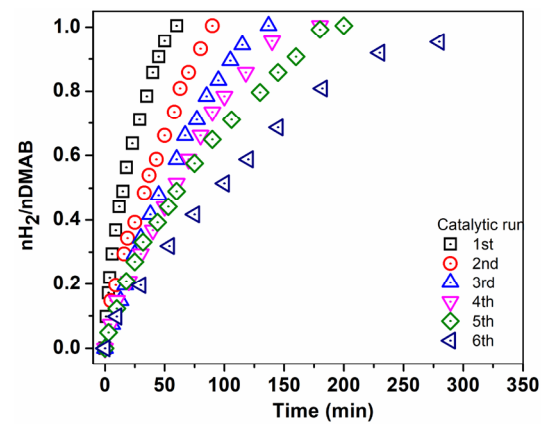

Figure 8. Catalytic performance of Pd^0/WO_3 in subsequent run of dehydrogenation.

micropipette. The solid and liquid part of the solution was tested separately in H_2 evolution reaction from DMAB. While the liquid part of the solution does not show any catalytic activity, the solid part retained its catalytic activity in the dehydrogenation reaction (Figure 9a). For the poisoning test, a typical experiment was started in the presence of 0.95 mM Pd catalyst at 60.0 ± 0.5 °C. After the liberation of 0.4 equiv H_2 from the dehydrogenation reaction, 0.2 equivalent of CS_2

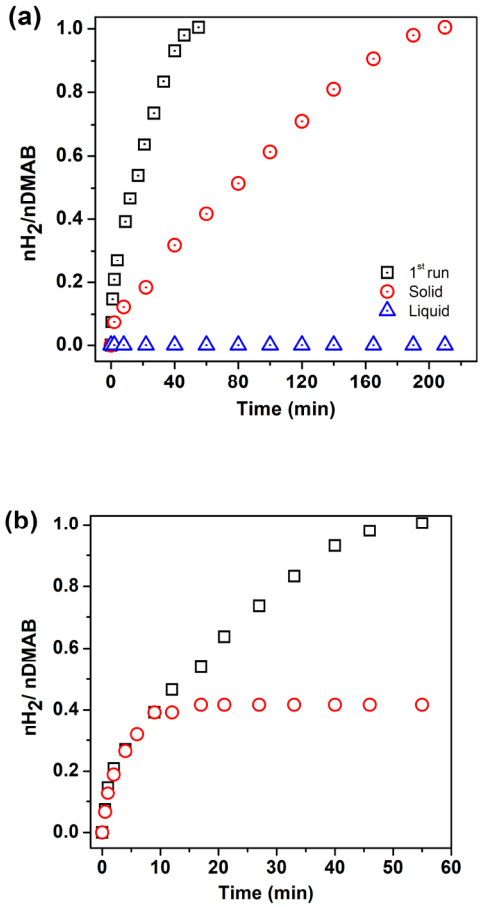

Figure 9. a) Leaching, b) Poisoning test for Pd^0/WO_3 NPs.

was injected into the reaction medium. The reaction stopped immediately after the addition of CS_2 due to the inhibition of the catalyst (Figure 9b). The result of leaching and poisoning tests reveal that catalyst is kinetically competent and dehydrogenation of DMAB is heterogeneous catalysis.

4. Conclusion

WO_3 supported Pd^0 NPs were obtained from the reduction of Pd^{2+} ions impregnated on the surface of WO_3 and tested as a catalyst in H_2 production from DMAB at 60.0 ± 0.5 °C. The results of the characterization techniques reveal that Pd^0 NPs are well dispersed on the surface WO_3 with an average particle size of 3.73 ± 0.58 nm. The initial TOF value reaches a maximum and decreases with the enhancement of Pd loading in the sample. The highest TOF value was obtained as 948.0 h^{-1} for 1.0% Pd wt. in Pd^0/WO_3 sample. The strong interaction between the WO_3 support and Pd NPs provides the high catalytic activity in H_2 evolution reaction. Especially reducible nature of WO_3 increases the recyclability of Pd^0 NPs in dehydrogenation reaction. Under reducing condition, WO_3 goes to a partial reduction of W6+ to W5+ ions on the surface as proved by observation of dark blue color. The excessive negative electron charge on the surface promotes the metal-support interaction. The facile preparation of Pd^0/WO_3 NPs and catalytic performance in dehydrogenation reactions make them a potential candidate to be utilized in H_2 releasing using DMAB as a solid hydrogen storage material.

References

1. Graetz J. New approaches to hydrogen storage. Chemical Society Reviews 2009; 38: 73–82. doi: 10.1039/B718842K

2. Metin O, Sahin S, Ozkar S. Water-soluble poly(4-styrenesulfonic acid-co-maleic acid) stabilized ruthenium(0) and palladium(0) nanoclusters as highly active catalysts in hydrogen generation from the hydrolysis of ammonia-borane. International Journal of Hydrogen Energy 2009; 34 (15): 6304-6313. doi: 10.1016/j.ijhydene.2009.06.032

3. Muradova TN, Veziroğlu NZ. From hydrocarbon to hydrogen–carbon to hydrogen economy. International Journal of Hydrogen Energy 2005; 30: 225-230. doi: 10.1016/j.ijhydene.2004.03.033

4. Staubitz A, Robertson APM., Manners I. Ammonia-borane and related compounds as dihydrogen sources. Chemical Reviews 2010; 110 (7): 4079–4124. doi:10.1021/cr100088b

5. Van den Berg AWC, Arean CO. Materials for hydrogen storage: current research trends and perspectives. Chemical Communication 2008; 6: 668-681. doi: 10.1039/b712576n

6. Staubitz A, Robertson APM, Sloan ME, Manners I. Amine and phosphine borane adducts: New interest in old molecules. Chemical Reviews 2010; 110 (7): 4023–4078. doi: 10.1021/cr100105a

7. Jaska CA, Temple K, Lough AJ, Manners I. Transition metal-catalyzed formation of boron−nitrogen bonds: catalytic dehydrocoupling of amine-borane adducts to form aminoboranes and borazines. Journal of American Chemical Society 2003; 125: 9424-9434. doi: 10.1021/ja030160l

8. Jaska CA, Temple K, Lough AJ, Manners I. Rhodium-catalyzed formation of boron–nitrogen bonds: a mild route to cyclic aminoboranes and borazines. Chemical Communication 2001; 11: 962-963. doi: 10.1039/b102361f

9. Turner J, Sverdrup G, Mann MK, Maness PG, Kroposki B et al. Renewable hydrogen production. International Journal of Energy Research 2008; 32 (5): 379-407. doi: 10.1002/er.1372

10. Karaboğa S, Özkar S. Ceria supported ruthenium nanoparticles: Remarkable catalyst for H2 evolution from dimethylamine borane. International Journal of Hydrogen Energy 2019; 44 (48): 26296-26307. doi: 10.1016/j.ijhydene.2019.08.103

11. Tanyildizi S, Morkan I, Özkar S. Ceria supported copper(0) nanoparticles as efficient and cost-effective catalyst for the dehydrogenation of dimethylamine borane. Molecular Catalysis 2017; 2: 57-68. doi: 10.1016/j.mcat.2017.03.002

12. Duman S, Özkar S. Oleylamine-stabilized copper(0) nanoparticles: an efficient and low-cost catalyst for the dehydrogenation of dimethylamine borane. International Journal of Hydrogen Energy 2017; 9: 2588-2598.

13. Zahmakıran M, Philippot K, Özkar S, Chaudret B. Size-controllable APTS stabilized ruthenium(0) nanoparticles catalyst for the dehydrogenation of dimethylamine-borane at room temperature. Dalton Transactions 2012; 41: 590-598.

14. Sen B, Demirkan B, Savk A, Kartop R, Nas MS et al. High-performance graphite-supported ruthenium nanocatalyst for hydrogen evolution reaction. Journal of Molecular Liquids 2018; 268: 807-812.

15. Yurderi M, Bulut A, Zahmakıran M, Gülcan M, Özkar S. Ruthenium(0) nanoparticles stabilized by metal-organic framework (ZIF-8): Highly efficient catalyst for the dehydrogenation of dimethylamine-borane and transfer hydrogenation of unsaturated hydrocarbons using dimethylamine-borane as hydrogen source. Applied Catalysis B-Environmental 2014; 160: 534-541.

16. Karaboga S, Özkar S. Nanoalumina supported palladium(0) nanoparticle catalyst for releasing H2 from dimethylamine borane. Applied Surface Science 2019; 487: 433-441.

17. Gülcan M, Zahmakıran M, Özkar S. Palladium(0) nanoparticles supported on metal organic framework as highly active and reusable nanocatalyst in dehydrogenation of dimethylamine-borane. Applied Catalysis B-Environmental 2014; 147: 394-401. doi: 10.1016/j.apcatb.2013.09.007

18. Sen B, Aygun A, Okyay TO, Savk A, Kartop R et al. Monodisperse palladium nanoparticles assembled on graphene oxide with the high catalytic activity and reusability in the dehydrogenation of dimethylamine-borane. International Journal of Hydrogen Energy 2018; 43: 20176-20182. doi: 10.1016/j.ijhydene.2018.03.175

19. Acidereli H, Cellat K, Calimli MH, Sen F. Palladium/ruthenium supported on graphene oxide (PdRu@GO) as an efficient, stable and rapid catalyst for hydrogen production from DMAB under room conditions. Renewable Energy 2020; 161: 200-206. doi: 10.1016/j.renene.2020.07.105

20. Sen B, Aygun A, Savk A, Calimli MH, Gulbay SK et al. Bimetallic palladium-cobalt nanomaterials as highly efficient catalysts for dehydrocoupling of dimethylamine borane. International Journal of Hydrogen Energy 2020; 45: 3569-3576. doi: 10.1016/j.ijhydene.2019.01.215

21. Sen B, Kuzu S, Demir E, Akocak S, Sen F. Monodisperse palladium-nickel alloy nanoparticles assembled on graphene oxide with the high catalytic activity and reusability in the dehydrogenation of dimethylamine-borane. International Journal of Hydrogen Energy 2017; 42: 23276-23283. doi: 10.1016/j.ijhydene.2017.05.113

22. Sen B, Kuzu S, Demir E, Yildirir E, Sen F. Highly efficient catalytic dehydrogenation of dimethyl ammonia borane via monodisperse palladium-nickel alloy nanoparticles assembled on PEDOT. International Journal of Hydrogen Energy 2017; 42: 23307-23314. doi: 10.1016/j.ijhydene.2017.05.115

23. Sen B, Demirkan B, Savk A, Gulbay SK, Sen F. Trimetallic PdRuNi nanocomposites decorated on graphene oxide: A superior catalyst for the hydrogen evolution reaction. International Journal of Hydrogen Energy 2018; 43: 17984-17992.

24. Barczuk PJ, Tsuchiya H, Macak JM, Schmuki P, Szymanska D et al. Enhancement of the electrocatalytic oxidation of methanol at Pt/Ru nanoparticles immobilized in different WO3 matrices. Electrochemical and Solid-State Letters 2006; 9 (6): E13-E16.

25. Rutkowska IR, Wadas A, Kulesza PJ. Mixed layered WO3/ZrO2 films (with and without rhodium) as active supports for PtRu nanoparticles: enhancement of oxidation of ethanol. Electrochimica Acta 2016; 210: 575-587. doi: 10.1016/j.electacta.2016.05.186

26. Baertsch CD, Komala KT, Chua YH, Iglesia E. Genesis of brønsted acid sites during dehydration of 2-butanol on tungsten oxide catalysts. Journal of Catalysis 2002; 205: 44-57. doi: 10.1006/jcat.2001.3426

27. Akbayrak S, Tonbul Y, Ozkar S. Tungsten(VI) oxide supported rhodium nanoparticles: Highly active catalysts in hydrogen generation from ammonia borane. International Journal of Hydrogen Energy 2021; 46: 14259-14269. doi: 10.1016/j.ijhydene.2021.01.156

28. Akbayrak S. Decomposition of formic acid using tungsten(VI) oxide supported AgPd nanoparticles. Journal of Colloid and Interface Science 2019; 538: 682-688. doi: 10.1016/j.jcis.2018.12.074

29. Liao C, Huang C, Jeffrey, S. Wu. Hydrogen Production from Semiconductor-based Photocatalysis via Water Splitting, Catalysts 2012; 2: 490–495. doi: 10.3390/catal2040490

30. Tressaud A, Khairoun S, Touhara H, Watanabe N. X-ray photoelectron spectroscopy of palladium fluorides Journal of Inorganic and General Chemistry 1986; 540: 291-299. doi: 10.1002/zaac.19865400932

31. Kim KS, Gossmann AF, Winograd N. X-ray photoelectron spectroscopic studies of palladium oxides and the palladium-oxygen electrode Analytical Chemistry 1974; 46: 197-200. doi: 10.1021/ac60338a037

32. Militello MC, Simko SJ. Palladium oxide (PdO) by XPS Surface Science Spectra 1994; 3: 395-401. doi: 10.1116/1.1247784

33. Laidler KJ. Chemical kinetics (3rd ed.). New York, USA: Harper & Row publishers, 1987.